# Elasticity and plasticity : foams near jamming

Siemens, A.O.N.

Chapter 3

# 2D Foams in a Wedge Geometry: Set-up

In this Chapter we describe the experimental setup that we have developed for probing the jamming transition in 2D foams. We use a bidisperse 2D foam packing consisting of bubbles sitting under a glass plate, like in [4, 5, 9, 10]; the glass plate helps to stabilize the foam, and eliminates the capillary attractions that arise for freely floating bubbles, thus allowing us to probe very wet foams and approach the jamming transition closely.

In our set-up, we confine our foam into a wedge geometry, which consists of two fixed and one freely rotating wall, forming a "pizza-slice" geometry. The rotating wall is connected to a rheometer, which allows us to control the imposed strain on the foam. In particular, it allows us to both compress and shear the foam. At the same time, this rheometer also allows us to probe the resulting torques, which directly translate into the pressure in the foam. We also image the foam from above, using a standard CCD camera, thus tracking the rearrangements and motion in the bulk.

There should be no doubt that this is a challenging experiment. 2D foams are really soft and, particularly when close to unjamming, very fragile. We therefore have to resolve very small forces, which motivates our use of a rheometer to measure these. Moreover, these fragile foams have a sluggish response, necessitating long experiments, which in turn require a good long term stability of the experiment; in particular, we have to stabilize the temperature, and make sure that coalescence and coarsening, intrinsic to foams, are minimized.

This chapter gives a detailed description of the experimental set-up that we developed. In Sec. 3.1 we first explain the rheometer geometry, how we make the foam, control the temperature and image the set-up. In Sec. 3.2,

we show how we adjust the tilt of the glass plate, and experiments on drifting bubbles, which give us important information of how the packing will behave under certain tilts we will impose to collect our data. Finally, in Sec. 3.3, we describe the protocols with which we compress the foam packing, and how the system behaves with varying compression and sit times.

## 3.1 Experimental Set-up

In this section we describe the set-up that we constructed to probe the jamming transition in two-dimensional foams. The main idea is illustrated in Fig. 3.1: a two-dimensional foam, consisting of a single layer of bubbles, floating on a surfactant solution and trapped below a glass plate, is kept in a wedge shaped area. Two side walls of the wedge are fixed, the third is mounted on a central axis, and acts as a wiper. By rotating the central axis, we can compress or decompress the foam. The axis is coupled to a rheometer, allowing accurate mechanical measurements of the foam. In parallel to these mechanical measurements, we image the foam from above, allowing us to follow and characterize the motion of the bubbles under compression.

The foam bubbles we use are between $2 - 4\,mm$ in diameter and even for compressions between about $10^{-7}\,m$ and $10^{-4}\,m$, the bubbles have a effective spring constant of $0.02\,Nm^{-1}$ and $0.075\,Nm^{-1}$, respectively [42]. This means they are very soft, and that the forces involved in compressing our two-dimensional foams are tiny. We therefore control the rotating of the wiper by a rheometer, allowing us to measure torques as small as $0.5\,\mu Nm$ with an angular resolution better than $1\,\mu rad$. By rotating the wiper we can thus both compress and measure the elastic response of the foam.

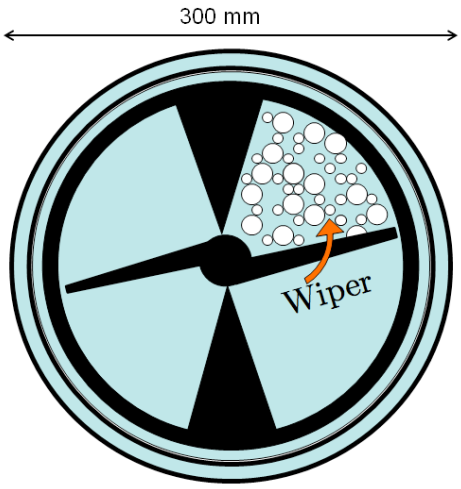


**Figure 3.1** – A top view schematic of the compression dish with black aluminum frame. The wiper is the third and only moveable wall of the wedge-shaped area the bubbles are confined to under the glass plate. A shaft connects the rheometer (sitting out of the plane) and the wiper, which imposes strain steps to compress the foam.

Since we wish to approach the jamming transition in these two-dimensional foams as close as possible, there are numerous experimental issues that need to be resolved, including stability of the foam, temperature control, and leveling. The outline of this section is as follows. We will first describe the set-up's components and how they are put together to create the wedge in which the foam is kept in Sec. 3.1.1. In Sec. 3.1.2 we describe the process of making the soap solution and how the bubbles are made. Additionally, we describe the way in which the foam is loaded into the experiment. In Sec. 3.1.3 we explain how the set-up is kept at a constant temperature during the course of an experiment. Then, in Sec. 3.1.4 we describe how we image the foam packing from above. Additionally, we highlight imaging techniques applied before analysis can be done.

### 3.1.1 Set-up

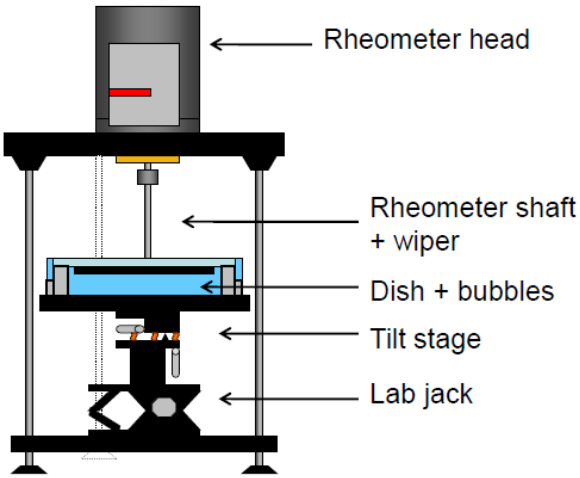


**Figure 3.2** – A side view of the bulk compression experiment. The rheometer shaft is attached to a wiper which can compress the bubbles under the glass plate. Leveling can be done with the tilt platform. A close-up of the dish which contains the foam solution and bubbles is presented in Fig. 3.3.

The set-up, Fig. 3.2, is composed of the main "dish", which holds the foam solution, the glass plate and the bubbles. The dish is circular, 300 $mm$ in diameter with an inner diameter of 250 $mm$ and 40 $mm$ deep, cut from a block of PMMA, see Fig. 3.3(D). An anodized piece of aluminum creates the boundaries of the sample cell and sits submerged in the cut-out area of the dish, as seen in Fig. 3.3(C) and Fig.3.1. An anodized "wiper" comprises the compressing face of a wedge shaped area the bubbles are trapped in and is attached to the rheometer by a shaft, which sits out of plane of the set-up, Fig. 3.4. We use an Anton Paar DSR 301 rheometer, which can be used in stress controlled mode and by a feedback mechanism, in strain controlled mode.

The wiper is 107.5 $mm$ long and has an effective edge length of 97 $mm$ to enclose the foam. There is a gap of 1 $mm$ between the tip of the wiper and the anodized aluminum frame, which is small enough to ensure that no bubbles can escape the wedge area under compression.

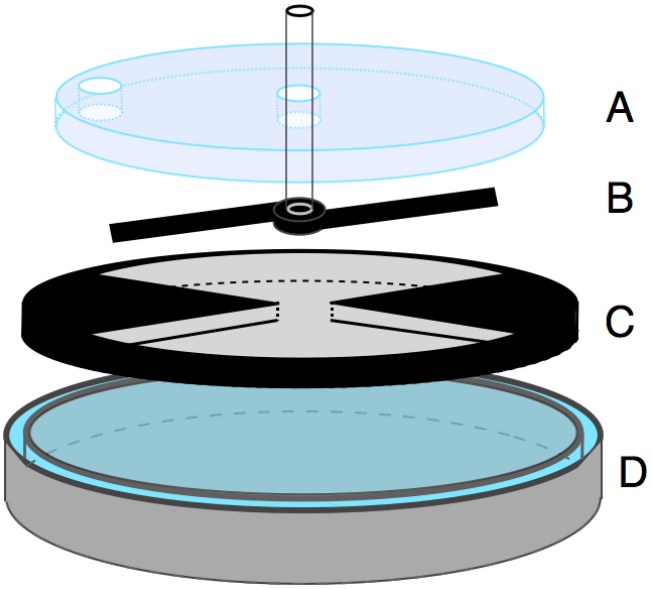


**Figure 3.3** – Schematic of the dish and other components. From top to bottom: the glass plate (A) with the anodized wiper (B), the anodized aluminum frame which creates the boundary of where the foam sits (C) and the PMMA dish that holds the soap solution (D). The bubbles sit under the glass plate, confined by the aluminum frame (C). The wiper's shaft is connected to a rheometer, which rotates the wiper, as is shown in Fig. 3.1. The dish (D) contains the soap solution and has an outside reservoir (shown as a blue-colored ring) from which solution can be extracted to enable the loading of bubbles through the perimeter hole on the glass plate, as described in Sec. 3.1.2.

The dish sits on a tilt platform that can be lowered to allow the sample to be replaced, as described in Sec. 3.1.2 and Sec. 3.2. The tilt platform is comprised of a Newport M-37 Tilt and Rotation platform mounted on a Newport 281 High Load Lab Jack.

Additionally, the experiment is isolated from vibrations of the ground, by being placed on an optical table.

The glass plate under which the bubbles sit is made from 10 $mm$ thick plain window glass and is 260 $mm$ in diameter. This window glass was first ground and then polished by a manufacturer, accurate to about 0.02 $mm$ /300 $mm$ (14 arcsec), see Fig. 3.5 a). We use this specially milled glass plate since normal glass panes are not flat enough and lead to drift of the bubbles sitting under it because of the "sagging" of the glass plate, as well as holes in the packing, as can be seen in Fig. 3.5b). The flatness is required so that the bubbles do not get "pinned" in place by impurities on the glass

surface. In Sec. 3.2.1 we test whether the polished plate is indeed flat. We find that it is very flat and that there is hardly any pinning left.

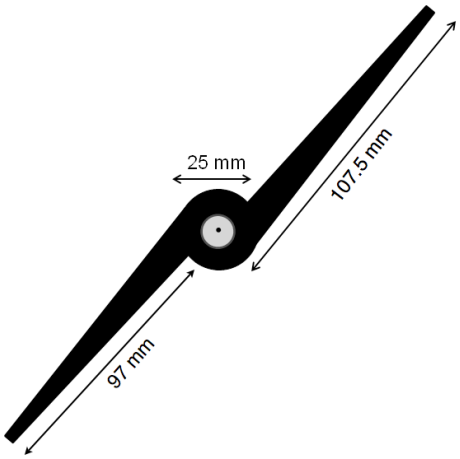


**Figure 3.4** – Top view schematic of the anodized, aluminum wiper. The effective edge of length 97 $mm$ compresses the bubbles under the glass plate. The wiper creates the third wall of the wedge-shaped area the bubbles are confined to under the glass plate. A shaft connects the wiper to the rheometer, which sits out of the page.

The plate has two holes of 17 $mm$ diameter, one around the edge and one in the center through which the wiper shaft is placed. The plate is placed on top of the aluminum frame and thus encloses the entire foam, as seen in Fig. 3.3. Once all pieces are placed together, the foam solution is poured into the dish. During this process, air bubbles become trapped under the glass plate and are removed by rotating the plate in such a way that the hole at the perimeter provides the escape.

Once all excess air bubbles are removed, a bidisperse foam can be loaded into the cell.

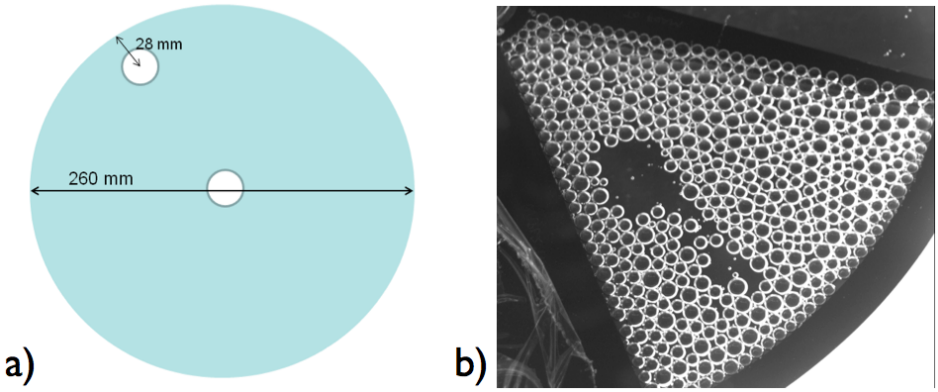


**Figure 3.5** – a) A schematic of the glass plate. The plate is made from 10 $mm$ window glass, yet one side under which the bubbles sit is machine polished to achieve a flatness of roughly 14 arcsec. The holes have a diameter of 17 $mm$. In b) we see how a packing is effected due to unevenness of a non-polished glass plate (before it was ground and polished): the glass plate "sags", causing the packing to drift away from these areas.

### 3.1.2 Foam

To approach the jamming transition by compression we must ensure that the sample does not crystallize. Especially in two-dimensional systems, this will occur readily in monodisperse systems. We therefore follow a well-known protocol used in numerical simulations [13] and use bubbles of two different sizes. The bubbles are about 2 and 4 $mm$ in diameter, measured by image analysis.

The foam solution is made according to the recipe in [43]. It is created in a two step process: first, a solution with total surfactant concentration of 10% consisting of 6.6 $wt\%$ anionic surfactant sodium lauryl esther sulphate (SLES) and 3.4 $wt\%$ zwitterionic surfactant cocamidopropyl betaine (CAPB) is added to 540 $mL$ demineralized water and stirred on a stir plate without heat. This is stirred until the SLES is completely dissolved, since it has a very viscous, wax-like texture. At the same time a stock mixture of 6.84 $L$ of demineralized water and 4.56 $L$ glycerol solution is made and shaken violently by hand to ensure that the glycerol has mixed properly with the water. The two solutions are mixed together by carefully pouring the high concentration surfactant mixture into the water/glycerol mix, since any shaking causes a lot of foaming. The water/glycerol phase dilutes the surfactant solution 20 times. Batches of 12 $L$ are made at a time in this way, and about 1.5 $L$ is used for any given experiment.

The final soapy solution is comprised of 0.33 $wt\%$ SLES and 0.17 $wt\%$

CAPB and has a glycerol concentration of 38 $wt\%$. The density of the solution is measured by pouring a known amount into a beaker on a scale. We find $\rho = 1094 \pm 2 \ \ kg\, m^{-3}$.

We measure the dynamic viscosity $\eta$ of the bulk solution with a Cannon Ubbelohde viscometer and find $\eta = 3.87 \pm 0.01\, mPa.s$. The surface tension, $\sigma$, was measured using the pendent drop method: a droplet of solution is suspended from an 18G ($0.84mm$ inner diameter) syringe and the curvature is measured, according to [44]. From this the surface tension is extracted. We find $\sigma = 26.5 \pm 0.3\, mN.m^{-1}$.

The foam is made separately in a petri dish by blowing $N_2$ gas at a constant rate through a needle submerged 20 $mm$ deep in the solution. The base pressure of the gas is $3.5 bar$, but decreased and tuned to useable levels using valves. To control the two different bubble sizes, we use two different gauge needles, 21G and 25G (0.51 $mm$ and 0.26 $mm$ inner diameters, respectively). We create about 50% big bubbles and 50% smaller bubbles by number.

The foam is then ladled with a spoon into the hole at the perimeter of the glass plate, which can be seen in Fig. 3.5. By extracting solution around the open, outer ring of the dish, see Fig. 3.3, an under pressure is created, which allows the bubbles to be "sucked" under the glass plate. The level of the solution never drops below the bottom of the glass plate. During this process, many small, unwanted bubbles are created, as seen in Fig. 3.6 a). The small bubbles cause problems during an experimental run in that they create slip-planes along which rearrangements can happen in a sample that would be otherwise in equilibrium. Additionally, these "satellite" bubbles under high compression coalesce with other bubbles in the packing, further bringing the packing out of its equilibrium state. They are removed by use of a bent syringe, which is fed in through the hole along the perimeter of the glass plate. This is also an effective means of ensuring, by eye, one last time that the packing does not have any crystalline patches or an overabundance of big or small bubbles before we enclose the set-up, see Sec. 3.1.3. Part of a "clean" packing without unwanted satellite bubbles or crystalline patches is shown in Fig. 3.6 b).

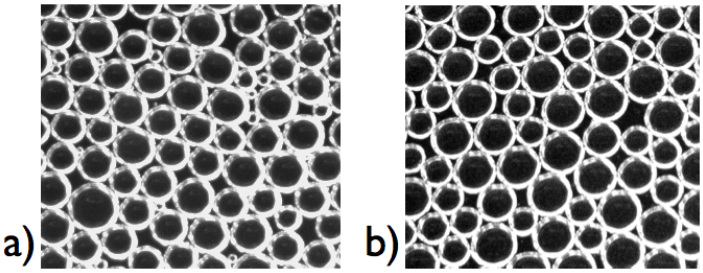


**Figure 3.6** – a) A zoom in of a packing of bubbles showing many small, unwanted "satellite" bubbles created when loading the compression cell. These small bubbles can sit in the Plateau boarders of larger bubbles and in the course of an experiment be the sources of slip-planes, which lead to rearrangements when there would normally have been none. Additionally, if the compression is high enough, these small bubbles can coalesce with others, further disrupting a packing in equilibrium. b) Part of a clean packing without satellite bubbles. The small bubbles are removed with a bent syringe needle.

Newly loaded samples are stable for about one to two days, meaning the likelihood of coalescence events, even under high compression, is rather low. However, after this time the foams rapidly lose their usefulness, since coalescence dominates their behavior. Coalescence means two bubbles which are pushed together merge into one big bubble due to the rupture of the film separating them. These merging events can be observed in the torque signal of the rheometer, mostly at low compressions, since the change in area causes the wiper to measure a torque different than before. In Fig. 3.7 we see how the torque measured by a coalescence event changes. There is a sharp spike due to the actual event before the system relaxes to a new equilibrium.

It is easy to identify two bubbles merging as shown in Fig. 3.7. When two bubbles of the same radius $R$ merge, the area increases by a factor of $2^{2/3}$. The subsequent rearrangements in the sample and drop in torque signal can be explained by a voronoi-type argument: it is the change in the number of neighbors before and after the coalescence event that determines the change in torque signal. As shown in Fig. 3.7, the peak in the torque signal is due to the actual creation of the larger bubble, but the noticeable drop in the torque signal comes from the number of neighbors changing with the new bubbles. The system must rearrange itself to keep a stable configuration. This chain of events can lead to the packing not being stable for many hundreds of seconds, effecting even the next compression step from reaching an equilibrium. Coalescence events are certainly identifiable, yet also rare in our bubble packings.

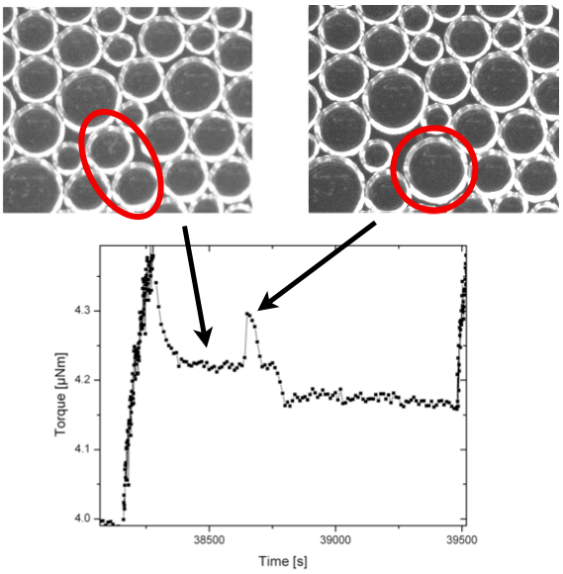


**Figure 3.7** – A coalescence event in the bulk of the packing and the corresponding change in the torque signal measured by the rheometer. The two consecutive images (top, left to right) show a coalescence event highlighted by the red circle. Two bubbles merge to become one due to rupture. Such events become more common the older the sample is. Note how after the event the relaxation profile (bottom) equilibrates to a lower torque than it was originally going to. This is due to the system rearranging itself to compensate for the newly created bubble.

At higher compressions the coalescence events are not picked up in the signal. However, we do know they occur occasionally by image analysis.

### 3.1.3 Temperature Control

Over the course of an experiment, which lasts several hours, the ambient temperature in the experimenting room varies depending on the outside weather. Direct sunlight coming through the windows in the summer or strong cooling over a winter night are main concerns. The fluctuation of the lab temperature can be as much as $5\,^{o}$C over the course of a day. Since the bubbles are made of $N_2$ gas, they are not impervious to these temperature fluctuations and will expand or contract depending on the ambient temperature.

By Charles's law

$$\frac{V_1}{T_1} = \frac{V_2}{T_2} \tag{3.1}$$

where $V_1$ is the volume of the bubble, $T_1$ the starting temperature, $T_2$ the

new temperature and $V_2$ the new volume of the bubble due to the variation in temperature. If the temperature changes by $5\,K$, as the lab temperature does on a hot, sunny summer day, $\Delta V = 1.6\%$.

However, to study the jamming transition, we need a precise control over the packing fraction, which necessitates accurate temperature control.

To help do this, the whole experiment sits inside a white polystyrene box of $100\,cm \times 80\,cm \times 80\,cm$. Its walls are $10\,cm$ thick. The box is suspended from the ceiling of the lab and can be hoisted up and down over the experiment to enclose it completely. Fig. 3.8 b) shows the experiment enclosed by the polystyrene box. Additionally, a $3\,cm$ thick piece of polystyrene is used to isolate the set-up as much as possible from the steel plate that makes up the optical table top on which the set-up rests, see Fig. 3.8 a). The polystyrene is EPS 100-SE and was chosen because of its low conductivity of $\sim 0.036\,Wm^{-1}K^{-1}$. This way we insure that over longer periods of heating the better part of the heat created stays inside the box.

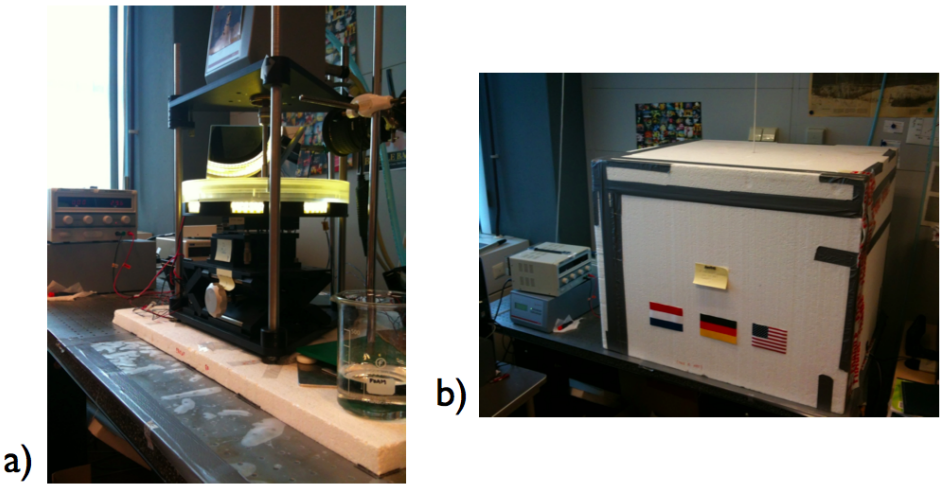


**Figure 3.8** – The experimental set-up. In a), the $3\,cm$ thick piece of polystyrene the set-up sits over is shown. This piece helps to thermally isolate the set-up from the metal table it sits on. In b), one can see the entire polystyrene box that is hoisted over the set-up to help maintain a constant temperature. The walls of the box are $10\,cm$ thick.

To heat the inside of the box we use two $5W$ heating elements connected in series, driven at $30\,V$. The heaters are connected to a Solid State Relay so that they can be switched on and off by a $5\,V$ signal controlled by a computer. Additionally, two large fans of diameter $10\,cm$ are placed inside

the box to circulate the air. One extra, smaller fan is placed in such a way that it blows over the LED lights (see Sec. 3.1.4) beneath the dish to ensure no heat is trapped under the set-up. It is imperative that no heat is trapped directly under the dish, since convection currents in the soap solution occur as a result of the heat. This in return effects the stability of the foam packing.

We control the temperature inside the box by way of a Product, Integral, Differential (PID) feedback loop. A PT-100 resistor (100 Ω resistance at 0 °C, ideally) at 10 $V$, 20 $mA$, wired in a Wheatstone bridge circuit is used to read in a voltage, $V_B$, measured across the two channels of the bridge, see Fig. 3.9. This measured voltage (the "process variable") corresponds to the measured air temperature inside the box.

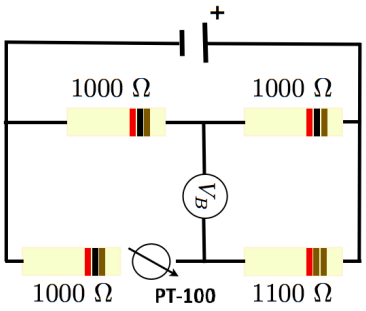


**Figure 3.9** – The Wheatstone bridge used for reading the bridge voltage in the circuit, $V_B$. This bridge voltage is called the process variable and is used in a LabVIEW code to measure the temperature inside the box. When the temperature changes, the PT resistor changes its resistance, changing the process variable.

This process variable is fed over a switchboard to a National Instruments PCI-6221 card to a LabVIEW code. The code then converts the voltage signal and determines the duty cycle of the heaters by way of the Solid State Relay so that a set-point temperature can be reached.

We set the set-point temperature close to 27.5 °C, above the ambient room temperature, since we can only heat the set-up. The precise temperature reached has to do with calibration of the PID loop and is not important, as long as it is above the ambient room temperature and is stable over long periods of time. The only temperature loss is due to the walls, which is very slow. The LabVIEW program ensures that if the temperature exceeds the set-point, the heaters are turned off and the system waits until the process variable sinks. However, the settings of the heaters that are controlled from the program are not strictly on/off. By use of the feedback, the program constantly reads the process variable and de-

termines a duty cycle: how much voltage the heaters need at any time to reach the set-point. The amount of time on or off is constantly updated until the set-point temperature is reached. By tuning the PID gain parameters, the program can approach the set-point faster or slower, with more or less overshoot or undershoot. We have managed to tune the parameters so that there is hardly any overshoot or undershoot, as seen in Fig. 3.10 a).

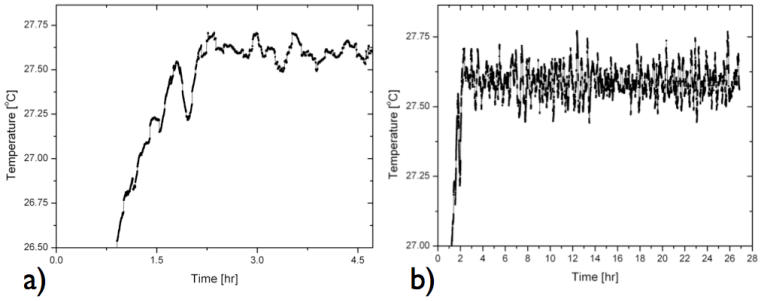


**Figure 3.10** – a) The process variable as a function of the time when heating the box. The set point is around 27.5 °C and the temperature quickly climbs to this value before fluctuating around it. The temperature reaches its set point without any major undershoot or overshoot. b) The temperature as a function of time for a full experimental run. The set point temperature is roughly 27.5 C. Here the temperature control ran for 27 hours without any major fluctuations from the set point, showing how well the temperature can be controlled by way of the PID loop.

It takes over an hour to bring the temperature inside of the box to the set-point of 27.5 C. During the long heat-up time, all components inside the box must also reach the set-point. Before this no measurement can be made on the foam. The temperature will then start to fluctuate around the set point temperature. The oscillations in Fig. 3.10 b) come from the PID constantly updating itself to fluctuations of the ambient temperature of the lab outside the box. If the temperature changes slowly, for instance when the evening cools down, the PID can account for these changes in the lab temperature.

The stability of the temperature is constant over long times, not varying by more than $\pm 30\,mK$ around the set-point, as is shown in Fig. 3.10 b). We can now see that, using Eq. 3.1, with the temperature varying no more than $\pm 30\,mK$, $\Delta V = 0.01\%$. This volume change is small enough that it can be ignored. It allows us to carry out our experiments sufficiently close to the jamming transition without having to worry about variations of the bubble volume over time.

One problem that arises when having such a “high” temperature inside

the box with air always circulating, is evaporation. Older experiments left the outer ring of the dish open to the air, as depicted in Fig. 3.3. Over the course of long experiments, the solution would evaporate from these parts and the level would sink. We would lose up to 30 $mL$ of solution this way per day. Not only do we lose solution, we also change the concentration of the surfactant in the solution. The lighter fluid, in this case the water, evaporates away, leaving behind more glycerol. This can lead to changes in the behavior of the foam. To address this problem, we place a petri dish with 100 $mL$ de-ionized water inside the box to keep the air humid. In addition, we place a circular rubber sheet over the exposed area on the perimeter of the pan. This way evaporation is reduced to a less than measurable amount.

### 3.1.4 Imaging

To observe the dynamics of our system under compression we film the set-up from above. The torque signal output by the rheometer can now be matched with rearrangements as well as coalescence events. The proper lighting of the foam is also crucial, since only with the light striking the Plateau borders at the right angle do the bubbles appear as discs when viewed from above.

The foam is lit from below at a slight angle by a strip of flexible LED (Silikon LED Flexstrip from SLV Elektronik GmbH) lights that sit directly under the dish, as seen in Fig. 3.11. The strip is bent into a circular shape and thus lights the entire dish from below. Imaging is done using a CCD camera (Basler A622f with $1280 \times 1024$ pixel resolution), equipped with a Sigma EXDG telephoto zoom lens. The leveling platform on which the dish sits is black, to enhance contrast, as in Fig. 3.11. The camera is triggered from a LabVIEW code and the frame rate is fixed at 0.1 $Hz$ or 0.033 $Hz$, depending on the compression protocol. The camera points along the x-axis onto a tilted mirror to film the set-up.

Due to the way the camera is filming the experiment we need to correct the images. The camera and mirror set-up do not image the bubbles exactly from above due to how they are placed inside the polystyrene box. From the front of the image to the back of the set-up is designated the y-axis, as shown in Fig. 3.16 b).

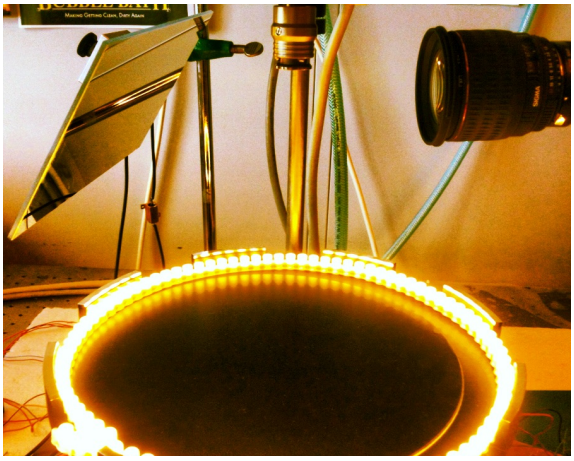

**Figure 3.11** – The camera (right) and mirror (left) placement above the tilt platform where the LED light strip lights the dish (not shown) from below. The lights are placed at a slight angle underneath the place where the foam packing will ultimately sit. The leveling platform is black to enhance contrast. Due to the tilt of the mirror over the dish and the alignment of the camera the images are skewed and will be corrected.

Similarly, the x-axis runs from left to right. The image is taken at a slight angle to normal, leading to the images being skewed. This means that a bubble seemingly becomes larger when it moves "closer" to the front of the image and shrinks when it moves towards the back. Parallel lines do not appear parallel, but splayed. To add to this, the direction of the x- and y-axis is not aligned with the image, since the camera does not point "exactly" along the x-axis.

We use a calibration image to correct the images as follows. The calibration image has a coordinate axis drawn on it that is aligned with the actual axis of the set-up. From this template grid, we map the correct coordinates on to any image of the bubble packing obtained by the camera using two IDL routines, POLYWARP and POLY_2D.

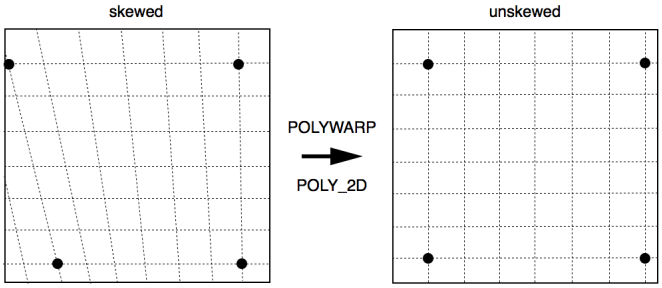


**Figure 3.12** – Cartoon of how POLYWARP and POLY_2D correct an image that is skewed. The black grid points are a guide to how the picture is corrected after the transformation.

POLYWARP determines rotation coefficients by performing polynomial spatial warping using tie points on the template grid to map to new coordinates on the rotated, skewed image, as illustrated in Fig. 3.12.

POLYWARP determines the polynomial coefficients $kx_{i,j}$ and $ky_{i,j}$ needed for image transformations from the polynomial functions:

$$x_i = \sum_{i,j} kx_{i,j} x_0^j y_0^i$$

$$y_i = \sum_{i,j} ky_{i,j} x_0^j y_0^i$$

The coefficients $kx_{i,j}$ and $ky_{i,j}$ are the inputs to the POLY_2D routine. The coordinates $x_i$ and $y_i$ are chosen from an image and correspond to some set of points $(x_0, y_0)$, set in advance from a calibration grid. Fig. 3.13 a) shows a calibration grid image from which $(x_0, y_0)$ and $(x_i, y_i)$ are extracted.

Next, we use POLY_2D, which performs the actual geometrical warping of the image with the rotation coefficients from POLYWARP above. The warping coordinates $(x', y')$ are determined as

$$x' = \sum_{i=0}^{N} \sum_{j=0}^{N} kx_{i,j} x^j y^i$$

$$y' = \sum_{i=0}^{N} \sum_{j=0}^{N} ky_{i,j} x^j y^i$$

Fig. 3.13b) shows the calibration grid image corrected after the POLY_2D routine has preformed the warping, using the coefficient inputs $kx_{i,j}$ and $ky_{i,j}$, determined by POLYWARP.

Since some pixels in the rotated image need to be padded due to the transformation, the POLY_2D routine performs an additional bilinear interpolation to decrease pixel noise. We could do this up to arbitrary order but use only linear order. Higher order means using more reference points, which is not necessary for our experiment. This method of image correction is used on all data sets before image analysis is preformed.

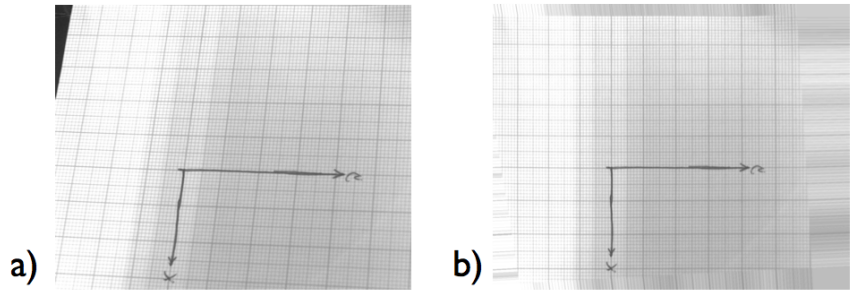


**Figure 3.13** – The calibration grid before, a), and after, b), the transformation done using two IDL routines, POLYWARP and POLY_2D. Shown is ruled, 1 $mm$ paper. Note how in a) parallel lines are splayed due to the skew of the camera's imaging. In b), one observes that the borders of the new image are stretched due to the transformation process. Only the inner part of the image showing the grid is of interest.

## 3.2 Leveling

While running the compression experiments, a leveling of the system presents itself as a very important issue. We have already tried to solve this by use of a polished glass plate. The leveling is fundamentally important in running any set of experiments since the motion of the bubble packing is very sensitive to the tilt of the glass plate with respect to gravity.

From jamming theory we have an idea of what our ideal scenario would be: the packing, under compression, should behave as a loose collection of bubbles in Fig. 3.14 a). That is, the bubbles initially sit under the glass plate, which in this scenario is mathematically perfectly flat, and are not touching. As we increase the packing fraction by decreasing the area they occupy, as we are doing in our compression experiments, they come together, touch and then pack together and deform. By this process one cleanly goes through the J-point, and measuring the elastic response would be an easy task.

However, this ideal scenario is a far cry from the actual situation when we preform experiments. It is impossible to *(i)* have a perfectly flat glass

plate and leveled system and *(ii)* create a packing of bubbles that sits in an initial configuration where no bubbles are touching.

We face the following problem: any experiment starts with a tilt that is not perfectly level. As a result, all bubbles in a packing are fully in contact. This means that the system starts out with a built-in stress due to the buoyancy of the bubbles pushing the packing into some configuration, due to tilt. The experiment is subject to continuous off-tilt of the glass plate in compressing our packing through the J-point. However, as outlined in points *(i)* and *(ii)* above, this is a Sisyphean task.

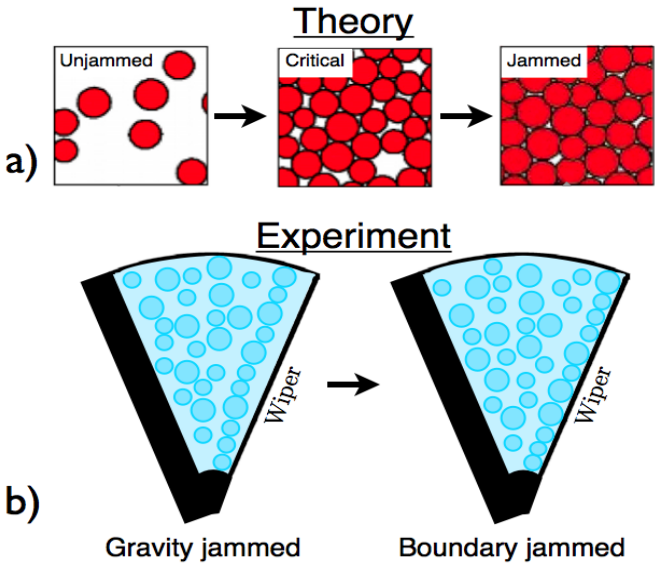


**Figure 3.14** – A comparison of theory and experimental approaches to foams. In a), a packing of bubbles goes through the jamming transition from an umjammed to a jammed state. In our experiments, as depicted in b), we start in a "gravity jammed" configuration with a hole between the packing and the wiper and compress until we are in the "boundary jammed" regime. Here the wiper has now closed the hole and is fully compressing the foam.

To counter these problems, we use the reality – that we can never perfectly level the system – to our advantage by purposely biasing the tilt. The bubbles now sit, due to our imposed tilt, in the wedge-shaped area. Furthermore, to draw parallels to the ideal scenario of going through the jamming transition, we tilt the bubbles into a configuration where a hole is created between the packing and the wiper, as in Fig.3.15. During compression, this hole is closed and the packing is said to undergo a transition from a "gravity jammed" (still weakly jammed due to the buoyancy gradient) to

a "boundary jammed" state, as shown in Fig. 3.14 b). We expect the torque signal to mark a clear difference between these two regimes, since in the gravity jammed scenario, the wiper is not fully compressing the system and thus not measuring the actual bulk modulus of the packing. Once the hole is closed and the packing is fully enclosed, the boundary jammed regime, we are measuring the compressibility of the foam.

Thus we have now a real world analog to the ideal, theoretical case of compressing a soft system. The results of using this approach are outlined in detail in Sec. 4.3.

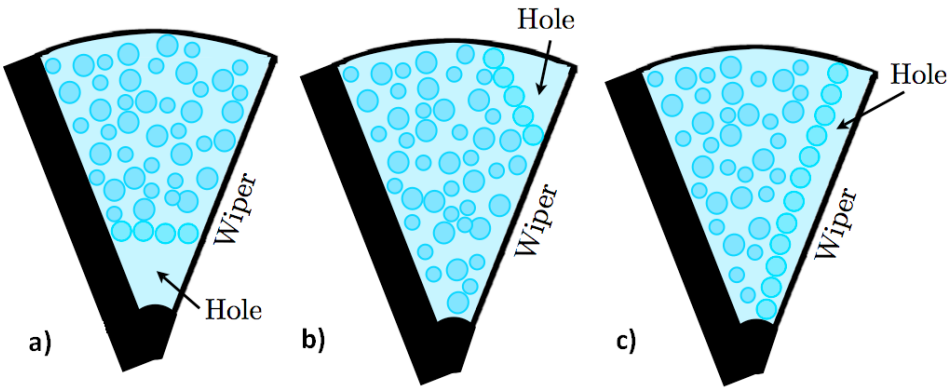


**Figure 3.15** – A cartoon of a number of different hole configurations used. Initial experiments with a biased tilt creating a hole in the packing were done, leading to versions a) and b). These experiments were improved upon once we saw that a cleaner signal was obtained by using hole configuration c), a hole running the length of the wiper axis.

The main dish holding the foam solution sits on top of a specially created leveling stage described in Sec. 3.1.1. The tilt platform uses two screws to adjust the tilt in the x- and y-direction. The screw is subtended into 50 "ticks". One full rotation is 0.5 $mm$. Thus, each tick changes the travel of the screw by 1/100 $mm$. The screws sit a distance of 89 $mm$ apart, which means that one full rotation tilts the platform by 5.61 $mrad$. Therefore, 1 tick = 0.11$mrad$. A schematic of the tilt platform is illustrated in Fig. 3.16 a).

Since the tilt can now be set very finely, we use a master orientation which tells us where the bubbles will move when we adjust the tilt screws. The convention uses the way the whole set-up sits on the optical table: from the front of the table to the back, going through the experiment if sitting in front of it, runs the y-axis. Again, sitting in front of the experiment, going left to right is the x-axis, as in Fig. 3.16 b). The screws can obviously

be turned clockwise or counter, so a convention needed to be created to distinguish the tilt. Turning either the x-axis or y-axis tilt screw to the left (clockwise if viewed from above) moves the side of the set-up closest to you *down*. A counter clockwise rotation would tilt the experiment *up*, as seen in Fig. 3.16 a).

Now that the orientation is established, we determine how bubbles move when changing the tilt *up* or *down*. In order to do that, we want to level the system as much as possible and determine the deviation from being flat. In Sec. 3.2.1 we check how flat the glass plate is, whether there is any pinning due to roughness and if the bubbles move smoothly in one direction, and that there is no deviations to a straight line due to sagging of the glass plate. We compare our estimates to a theoretical prediction established by Bretherton and others [45, 46, 47, 48] in Sec. 3.2.2.

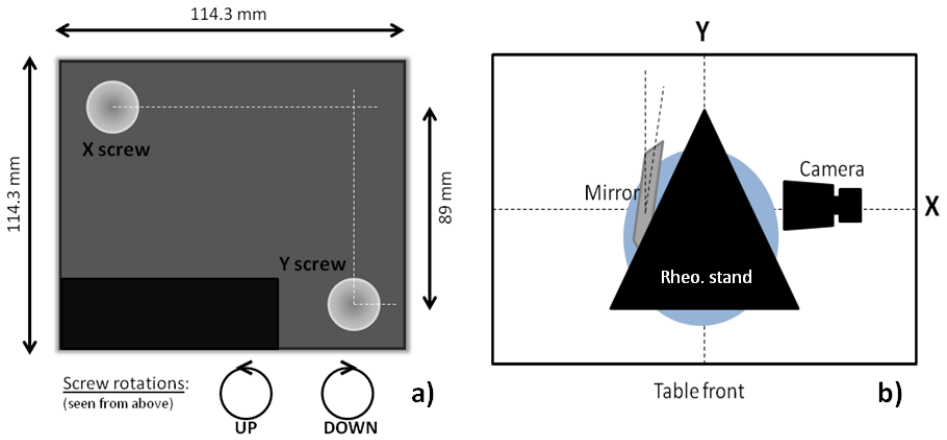


**Figure 3.16** – Schematics of the screw platform used for leveling the system, as well as the table top where the set-up sits on. a) A top view schematic of the tilt platform screw layout. A counter clockwise turn (seen from above) of either the X or Y screw turns the platform *up*. Clockwise turns it *down*. The dish with the bubbles is mounted on top of the tilt platform. b) Top view of the table. The tilt platform schematic and its actual orientation as seen when sitting in front of the set-up.

### 3.2.1 Protocol to Level

We create a protocol with which we probe different tilts on a single bubble under the glass plate. By looking at the motion we can then determine the direction of the bubble, if it moves in a straight line or deviates due to unevenness of the glass, and its velocity. We systematically change the

angle to create a velocity vector field of the bubble. The point where the velocity approaches zero gives us the best estimate where the tilt is minimal.

We start the experiment with a single bubble under the glass plate. This bubble is roughly $5\,mm$ in diameter, larger than the largest bubble we use in our bidisperse packings for the bulk compression experiments. The larger the bubble, the more sensitive it is to changes in the tilt. The bubble is not allowed to touch the boundaries of the cell, since we are interested in its free movement due to the tilt.

To start, some initial tilt settings for the axis were chosen around which we change the tilt. These are:

$$\begin{aligned} X: &\quad 6.5\,mm + 20/50\,mm \\ Y: &\quad 7.5\,mm + 49/50\,mm \end{aligned}$$

Here the notation $XX/50\,mm$ means that the tilt is at the $XX$'th tick out of 50 of the screw. These values are the fine-tuned adjustments we make to the tilt of the set-up.

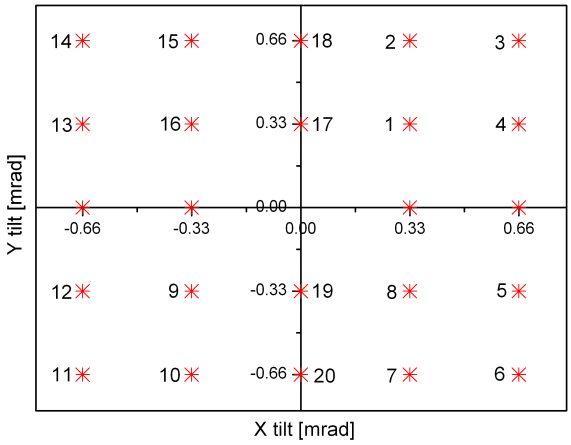


**Figure 3.17** – A grid showing the tilt coordinates probed as red stars. The center of the grid is the arbitrarily chosen initial tilt position. Moving along the positive x- or y-axis is *up*. Going into the negative ranges of the axis is *down* when turning the tilt screws. The numbers next to each star show in which order we changed the tilt. All points along the x-axis were done separately. This protocol produced Fig. 3.19.

We proceed by systematically changing the tilt according to a grid, see Fig. 3.17. Here we probe the tilt in steps of three ticks ($0.33\,mrad$) in either x- or y-direction. Three ticks are chosen since this causes the bubble to move enough in the 10 minutes we record the movement with the camera.

Once the time is up, we change the tilt to the next position on the grid and start filming again.

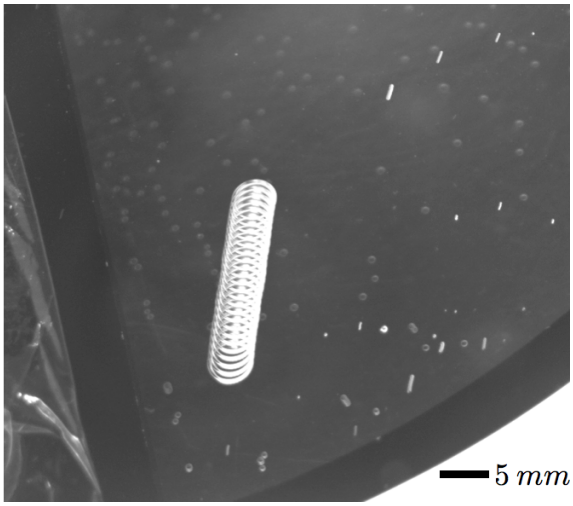


**Figure 3.18** – A superposition of images to show a bubble moving in a straight line under the glass plate. The bubble is roughly 5 $mm$ in diameter. The whole track movement is 1780 $sec$ long, 80 $sec$ between each white ring seen in the figure.

We ensure that the bubble does in fact move in a straight line, that the glass plate is without unevenness or local rough patches due to the grinding and polishing process described in Sec. 3.1.1, unlike what could be seen in Fig. 3.5 b). By analyzing the tracks (a track being the bubble movement due to an imposed tilt) of the bubble through the video images, we can convince ourselves that the bubble always moves in a straight line from the beginning of the imposed tilt until we change the tilt, as in Fig. 3.18.

Once all points on the grid have been covered we use ImageJ to piece together the tracks the bubble has traced out under the glass plate to measure the velocity. This can be seen in Fig. 3.19 and Fig. 3.20. We notice that several smaller bubbles in the set-up become pinned and do not trace out the full track, the way the big bubble does. The fact that most of the satellite bubbles do follow the same track shows us that the plate is very smooth.

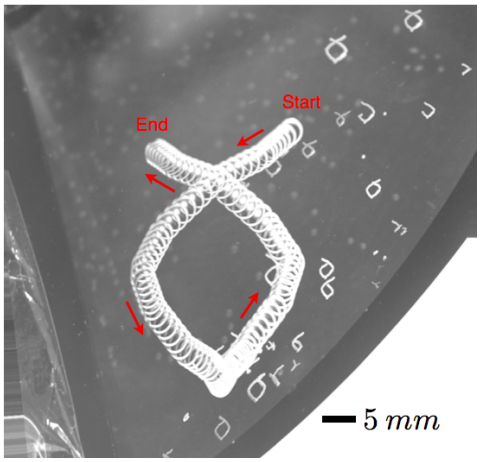


**Figure 3.19** – A superposition of the first 16 points in the grid of Fig. 3.17. The time between each ring is 100 seconds. The bubble is roughly 5 $mm$ in diameter. The image has been corrected for skew. By chance this ribbon-like bubble path was created. The start is the top right position, the end is the top left position.

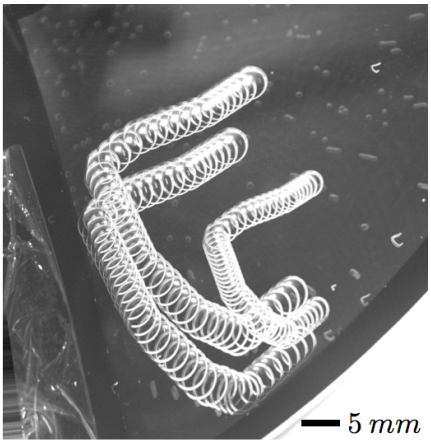


**Figure 3.20** – A superposition of three bubbles under the glass plate. The time between each ring is 10 seconds. The two larger bubbles at the top are roughly 5 $mm$ in diameter. The image has been corrected for skew. The start of the imposed tilt is at the top. The bubbles end up at the bottom. The smoothness of the glass plate is again highlighted by the much smaller bubbles also following the tilt motion of the glass plate.

### 3.2.2 Equilibrium Coordinates

We take the first and last image for any straight section of a track at a fixed tilt and find the center-point coordinate of the bubble. Knowing the time for each track and the coordinates, we can calculate the x- and y-velocity components for all points in Fig. 3.17, $(v_x, v_y)$. The result is shown in Fig. 3.21. The arrows show the magnitude and direction of the velocity of the bubble drift. The value of the velocity for each tilt as a function of the tilt is plotted in Fig. 3.22. In this case, the length of the arrows is increased by 100× to show their direction.

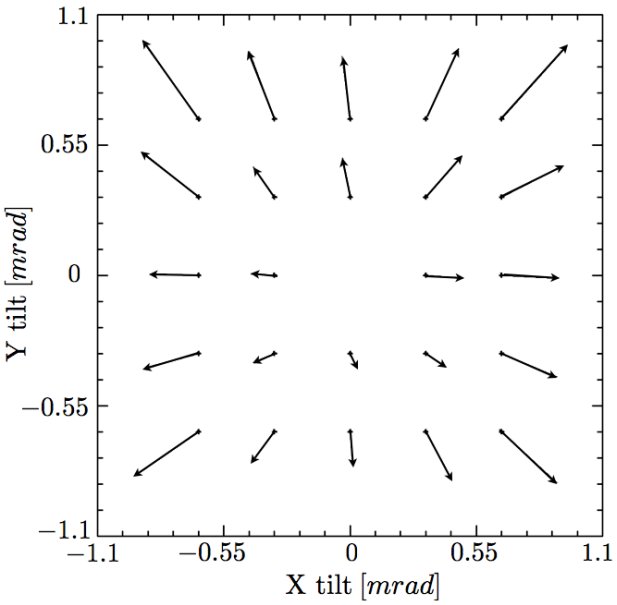


**Figure 3.21** – The velocity profile of the bubble at different tilt positions given by Fig. 3.17. As expected, the velocity is larger when the tilt is greater.

From the figure we note that our initial tilt settings are fairly good estimates of where zero tilt is, since all velocity vectors seem to originate at our initial setting. They are, however, not quite emanating from $(0, 0)$. We want to determine their origin position, $(x_0, y_0)$, as the tilt coordinates should be for a completely level system.

We define the directional vector from our to-be-determined origin where the tilt is zero, $\hat{r}$, to the coordinates that correspond to points picked for each tilt in Fig. 3.17. Here

$$\hat{r} = \frac{\binom{x-x_0}{y-y_0}}{\sqrt{(x-x_0)^2 + (y-y_0)^2}} \tag{3.2}$$

where the denominator is the length of the vector from $(x_0, y_0)$ to $(x, y)$ and can be seen as an angle between the origin and $(x, y)$.

The drag force (per unit length) on a bubble under a glass plate is related to its velocity by Bretherton's law as set forth in [47] $F = 4.70\sigma(Ca^\star)^{\frac{2}{3}}$, where $(Ca^\star) = \frac{\eta v}{\sigma}$ is the bubble-wall capillary number. Equating this with the buoyancy force a bubble of radius $R$ feels under an inclined plane of tilt angle $\theta$, $F = \frac{4}{3}\pi R^3 \rho g \times \sin\theta$, we can get the velocity of the bubble as a function of the tilt of our glass plate. Note that the force in the buoyancy equation is linearly proportional to the angle of tilt. If we now dot the velocity vector for every tilt, $\overrightarrow{v} = (v_x, v_y)$ in to $\hat{r}$, and plot this versus the angle, we can vary our estimated coordinates of $(x_0, y_0)$ to collapse all the data as much as possible.

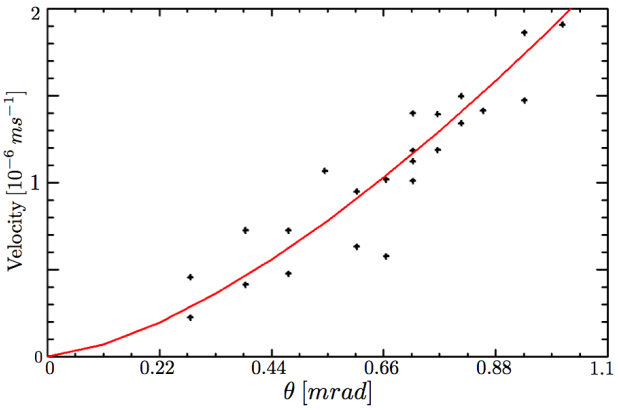


**Figure 3.22** – The velocity of a bubble moving under the glass plate versus the tilt. The line of best fit is in red.

If we calculate numerically the relation between the velocity as a function of the tilt, as described above, we get

$$v = 0.065\, ms^{-1} \times \theta^{1.5} \tag{3.3}$$

The line of best fit in Fig. 3.22 is $v = 0.07\, ms^{-1} \times \theta^{1.5}$, in excellent agreement. By only knowing the buoyant force and the velocity of a bubble under our glass plate, Fig. 3.22 shows that our bubbles are behaving like the ideal case proposed by Bretherton [45] of a bubble sitting under a flat plate.

## 3.3 Compression Protocols

In this section we describe the compression protocols we use to probe the jamming transition in our two-dimensional foam packing. The main idea is to compress the foam, trapped in the wedge of our set-up, by small, incremental strain steps and to measure its elastic response. The steps can be anywhere between $0.5 - 12\,mrad$, which for typical wedge openings in the order of $1\,rad$ corresponds to strains between $5 \times 10^{-4}$ and $10^{-2}$. As we will see in Fig. 3.26, the stress responds on a timescale of several minutes, and we choose relaxation times of the system between these steps from $400 - 1200$ seconds. We will show which combinations of step size and relaxation time give a well equilibrated response and thus allow us to measure the elastic moduli of the foam.

In Sec. 3.3.1, we show the difference between the angle measured by the rheometer and the open angle, measured by image analysis. Sec. 3.3.2 discusses the dynamics of the system and how by controlling the compression and sit times of the experiment, we ensure that the system is equilibrated. In Sec. 3.3.3 we give a detailed description of the different compression protocols used.

### 3.3.1 Deflection Angle vs. Open Angle

For all experiments, the open angle of the wedge and the deflection angle imposed by the wiper on the packing are of great importance. However, there are differences in obtaining and also in using these two in the data analysis.

The deflection angle, $\theta$, is the angle that the rheometer tells the wiper to move and change between protocols, as shown in Sec. 3.3.3. The starting point is arbitrarily set by the rheometer, meaning wherever the wiper sits at the start of any experiment is the designated reference point. Each subsequent step is measured from that reference point. For the protocols outlined below, only this deflection angle is used to compress the foam.

The open angle of the wedge geometry, $\theta_0$, is measured using ImageJ. By using the images of the foam after each compression step, we measure the angle between the static wall and the wiper. This allows us to calculate the area of the wedge during the entire run, which will be of use in the next chapter.

### 3.3.2 Dynamics of Different Protocols

These steps are characterized by three quantities: the change in angle between steps, $\Delta\theta$, the change time between steps, $t_c$, and the sit time at an angle, $t_s$. In all protocols, the wiper sits at one imposed angle before moving to the next one at a finite rate, as shown in Fig. 3.23. The change in angle, $\Delta\theta$, and $t_c$ are the same for all protocols outlined below, only $t_s$ is changed between different protocols. In our experiments, we use the rheometer in strain controlled mode, and during the step-wise compression, the torque from the bubbles on the wiper is measured.

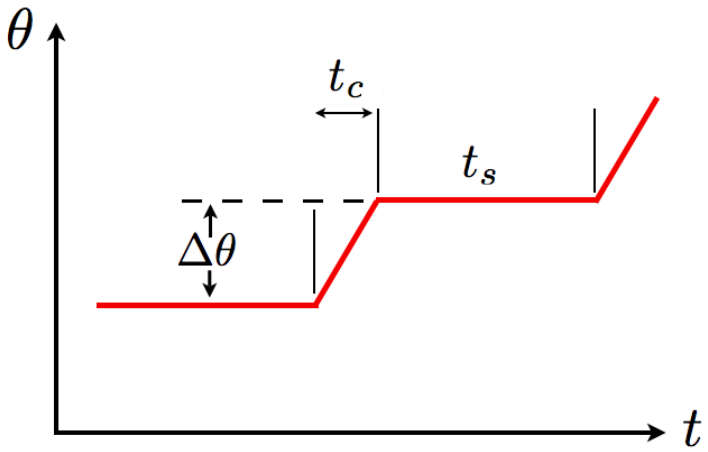


**Figure 3.23** – Sketch of the deflection angle versus time. The wiper moves linearly by a change in angle $\Delta\theta$ over time $t_c$ to the new angle, where it sits for time $t_s$.

We choose $t_c = 120$ seconds. The corresponding finite rate of change in angle prevents dynamic effects to dominate, such as the creation of little satellite bubbles in Fig. 3.6 a). Moreover, this rate is slow enough for the system to quasi statically move to be compressed; shorter $t_c$ disturbs the packing too much and in that case it takes the system far longer to reach an equilibrium during the sit time.

To allow the system to equilibrate after each compression step, we keep the wiper fixed for a duration $t_s$. Typical equilibration times, seen from the torque signal, range from several minutes for low compressions, like in Fig. 3.24 a), to tens of seconds for higher compressions, as in Fig. 3.24 b).

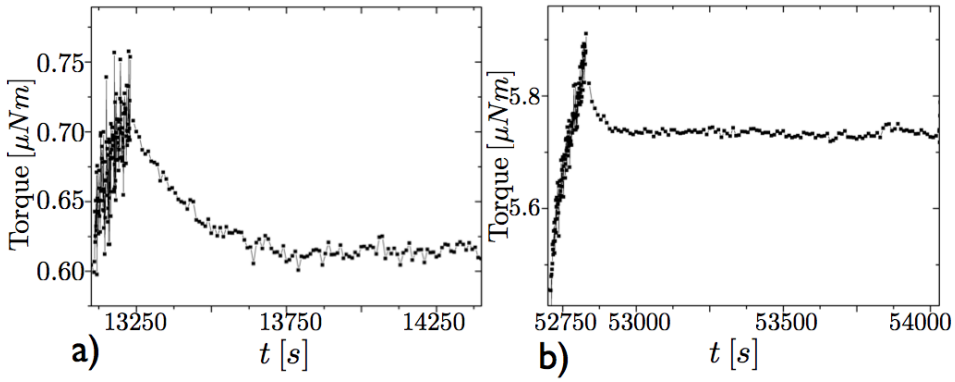


**Figure 3.24** – a) At lower torques, equilibration times can be several minutes. b) At higher compressions, equilibration happens much faster, over several tens of seconds.

For low compressions, rearrangements become more frequent, and depending on protocol, we take $t_s$ anywhere from 400 to 1200 seconds, allowing the system to equilibrate.

### 3.3.3 Stress vs Strain Control

The wiper, which makes up the third edge of the wedge in which the foam packing sits, see Fig.3.1, is attached to a shaft which is rotated by a rheometer. As mentioned in Sec. 3.1.1, the rheometer can be used in strain and stress controlled mode. We only use strain controlled mode, since the system relaxes faster than when using stress controlled protocols. Fig. 3.25 shows the difference between equilibration times for strain and stress controlled protocols. The difference between the two modes is astonishing: packings compressed using the strain controlled mode of the rheometer equilibrate within minutes (or even faster if very compressed), see Sec. 3.3.2 above, whereas for stress controlled mode, as in Fig. 3.25 b), the packings sometimes do not equilibrate at all.

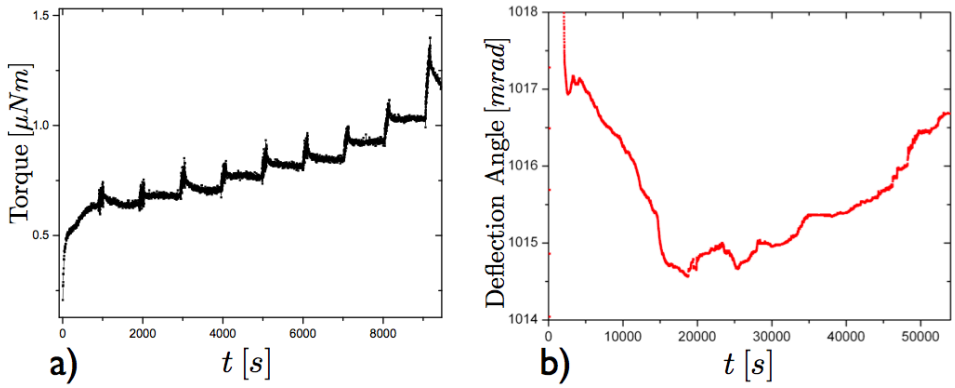


**Figure 3.25** – a) A zoom-in of a well equilibrated compression protocol using the strain controlled mode of the rheometer. b) A signal of the wiper compressing a sample in stress controlled mode over 15 hours. The rheometer measures the change in angle when a constant torque is imposed. Note how the system never equilibrates over the course of the imposed stress.

### 3.3.4 Protocols

We have explored three different strategies for leveling the system. Initially, we aimed at leveling the top plate to the best of our abilities: we call this the "flat" protocol. Then, we added a tiny but controlled tilt to the system, and oriented the tilt such that a hole formed in the foam close to a corner of the system: the "corner-hole" protocol. Finally, we settled on a protocol where the tilt is oriented such that gravity is approximately perpendicular to the wipers orientation, leading to a long stretched-out hole near the wiper: "slice-hole" protocol. Most data presented in the following chapter are obtained in the slice-hole protocol.

#### 3.3.4.1 Flat Protocol

The first problem one encounters in experiments on 2D foams below a top plate is the strong sensitivity on the residual tilt of this plate. The most natural approach is thus to level this top plate as well as possible, thereby reducing to the minimum the effect of buoyancy, which leads to drift of free bubbles. However, once one approaches the (un)jamming transition, a hole spontaneously forms somewhere near the boundaries. The hole's precise location is set by the orientation of the residual tilt. This hinders the interpretation of the jamming behavior in our foams. Nevertheless, for more strongly compressed foams such problems do not arise, and below, we describe the outcome of some of these explorations.

In Fig. 3.26 we used the flat protocol and probed almost two decades in torque, carefully staying away from the very low compression regime. Once the cell was loaded with bubbles, we lightly compressed the packing with a low torque of about $2-3\,\mu Nm$ to make sure all bubbles were in the wedge-shaped area. We turned off the torque and let the system relax and set the deflection angle of the wiper to constant, once we visually determined the packing to be stable and the torque signal to be sufficiently low. At this point we started the compression. The imposed deflection angle went (in $mrad$):

$$0, 0.5, 1, 2, 3, 4, 5, 6, 7$$

and then in steps of root two. After each step of root two, which we call the compression step, there was a "measurement" step, which is 1 $mrad$ more compressed, see Fig. 3.26.

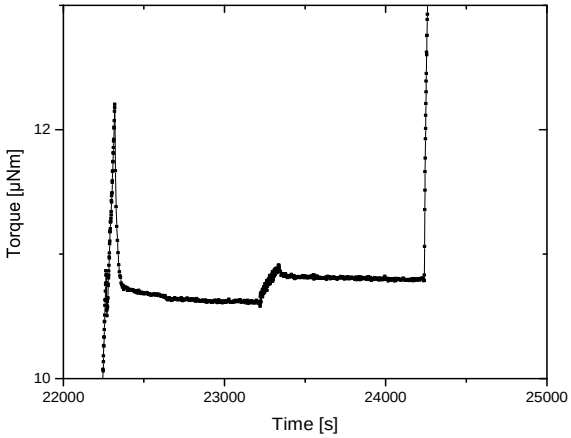


**Figure 3.26** – A compression step followed by its measurement step, which is 1 $mrad$ more compressed, used in the "flat protocol". The sit time for each step is 900 seconds.

The final deflection angle was 190 $mrad$ from the start point. The sit time at every angle was 900 seconds and the wiper changed angle linearly to the new angle in 120 seconds. The total strain range for this experiment was 24%, which for this system corresponded to a range of torque probed between $\lesssim 0.5\,\mu Nm$ to $75\,\mu Nm$. Fig. 3.26 shows full equilibration.

Although successful, we abandoned this flat protocol because it did not not allow us to get very close to jamming. For the lowest torques, a hole would open up in the foam packing, and the interpretation of the results

was somewhat opaque; in particular, it was now unclear where precisely the jamming transition takes place.

#### 3.3.4.2 Corner Hole Protocol

To control the location where the hole appeared when uncompressing the foam, we tuned the top plate so that it deviated from the horizontal by an angle of order 0.33 $mrad$, and orientated this residual tilt so that the hole in the foam opened up in a corner of the foam, see Fig. 3.15 b).

While this protocol allowed us to control the location of the hole, its location was such that a relatively large change in the wipers location was necessary to open or close the hole. Moreover, we observed that there was bridging in the foam right before the hole closed. The bubbles would move to close the hole. Before it could be enclosed completely by the wiper, the remaining bubbles at this point created a bridge, leading to higher than normal torque signals until the bridge disappeared due to a rearrangement only many steps later.

In Fig. 3.27 we show an example of such a run, performed for compression steps of 1 $mrad$ and sit time 400 seconds. We compressed a system with this type of hole for four different tilts of the glass plate, each time increasing the tilt by 3 ticks (0.33 $mrad$), tilting the glass plate a total of 1.32 $mrad$. The bridge can be seen in Fig. 3.27.

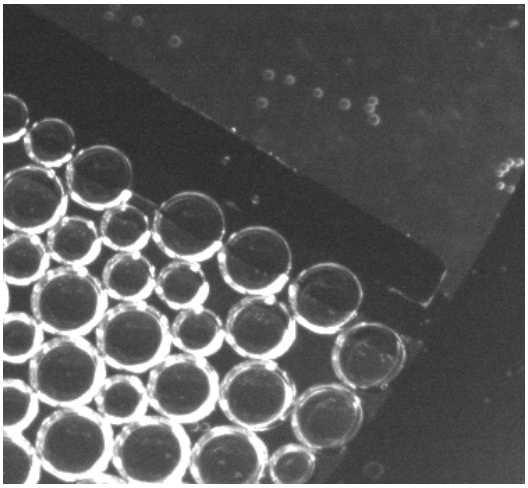

**Figure 3.27** – A pentagon arrangement of bubbles at the tip of the wiper during the "corner hole" protocol. This bridging happened repeatedly and with too many bubbles being in contact with the wiper at the start of an experiment led to us to abandon this protocol for the "slice hole" protocol.

We were thus not compressing the system fully, just measuring the response of the bridge. Also, the shorter sit time we used for this protocol showed that we were not letting the system relax long enough: the trend of the signal showed many times that the foam had not reached a relaxed state.

#### 3.3.4.3 Slice Hole Protocol

This protocol also uses a controlled tilt, now orientated so that the wiper lies parallel to the packing when a hole is formed; the slice hole ensures that there is no initial contact between the packing and the wiper. Ideally, the wiper closes the hole and makes contact with the sample at the same time along the length of the wiper; in practice we have limited control over the precise orientation of the tilt (as the absolute tilt angle is already very small), but we can orientate the tilt sufficiently well so that bridging is essentially absent. An example of the final configuration of the hole is shown in Fig. 3.15 c). This protocol yielded the clearest difference in torque signal between the gravity and the boundary jammed regions, and will be used in the following chapter.